Eur Biophys J (2002) 31: 331–340
DOI 10.1007/s00249-002-0223-5

ARTICLE

**Dietmar Uttenweiler · Wolfgang G. Kirsch
Erich Schulzke · Martin Both · Rainer H.A. Fink**

Model-based analysis of elementary Ca^{2+} release events in skinned mammalian skeletal muscle fibres

Received: 18 January 2002 / Revised: 7 March 2002 / Accepted: 8 March 2002 / Published online: 11 June 2002

Abstract Using high temporally and spatially resolved confocal laser scanning microscopy, we have recently demonstrated the existence of elementary Ca^{2+} release events (ECRE) in chemically and mechanically skinned fibres from adult mammalian skeletal muscle. Here, we present a first approach to the analysis of mammalian ECRE with a spatio-temporal mathematical model of Ca^{2+} ion distribution in skinned muscle fibre preparations. The differential equations for the main processes, including sarcoplasmic reticulum Ca^{2+} handling, are solved in a 2-D cylindrical geometry by the method of explicit finite differences. By calculating the various spatio-temporal ion concentrations as well as the theoretical fluorescence signals for confocal microscopy, corrected for the point spread function, the model output can be directly correlated with the experimental data. Thus, the basic features of mammalian ECRE were successfully reproduced with our model. In particular, under our model assumptions a considerable depletion of luminal free calcium is predicted even for short spark-like ECRE. For a full understanding of the molecular and sub-cellular events responsible for EC coupling it is vitally important to combine the experimental and modelling approaches to elucidate the contribution of mammalian ECRE to the global Ca^{2+} release and its alteration under various physiological and also pathophysiological conditions.

Presented at the Australian Biophysical Society Meeting, 2001

D. Uttenweiler and W.G. Kirsch contributed equally to this work.

D. Uttenweiler (✉) · W.G. Kirsch · E. Schulzke · M. Both
R.H.A. Fink
AG Medical Biophysics,
Institute of Physiology and Pathophysiology,
Ruprecht-Karls-Universität Heidelberg,
Im Neuenheimer Feld 326,
69120 Heidelberg, Germany
E-mail: dietmar.uttenweiler@urz.uni-heidelberg.de
Tel.: +49-6221-544063
Fax: +49-6221-544123

Keywords Calcium · Ca^{2+} sparks · Excitation-contraction coupling · Mathematical modelling · Sarcoplasmic reticulum

Introduction

The regulation of contractile force development in skeletal muscle is achieved by the voltage-dependent release of Ca^{2+} ions from the sarcoplasmic reticulum (SR), the intracellular Ca^{2+} ion store. This subsequently leads to an increase of the intracellular free Ca^{2+} ion concentration by up to two orders of magnitude, which activates the Ca^{2+} regulatory proteins and initiates contraction. The central mechanism of excitation-contraction (EC) coupling is the conversion of the electrical trigger signal, the action potential (AP), into the release of Ca^{2+} ions from the SR. In skeletal muscle this conversion is achieved by a direct mechanical interaction of the voltage-sensing dihydropyridine receptors [DHPR, located in the transverse tubular system (TTS) of the outer sarcolemma; Ríos and Brum 1987] with the Ca^{2+} release channels of the SR, the ryanodine receptors (RyR) (Dulhunty 1992). This mechanism is structurally based on the morphology of the triadic junction, where the TTS and the terminal cisternae of the SR are in very close contact, with every second ryanodine receptor in the SR membrane facing a tetrade of DHPR (skip pattern; Block et al. 1988) in the TTS. In addition to the voltage-dependent activation, RyR can be triggered to a lesser extent by Ca^{2+} ions via calcium-induced calcium release (CICR), which is the main trigger for calcium release in heart muscle (Lipp and Niggli 1998).

Using high-resolution confocal fluorescence laser scanning microscopy, elementary Ca^{2+} release events (ECRE) through single or clusters of RyR could be detected in heart (Cheng et al. 1993), smooth (Nelson et al. 1995), and amphibian skeletal (Tsugorka et al. 1995; Klein et al. 1996) muscle fibre preparations. However, so far, controversial results have been reported in mammalian skeletal muscle fibre preparations,

ranging from the non-existence of sparks in adult rat fibres under voltage clamp conditions (Shirokova et al. 1998) to a scarce appearance of sparks in intact adult mouse muscle fibres (Conklin et al. 2000). In a recent study (Kirsch et al. 2001) we have demonstrated the abundant existence of ECRE in adult mammalian skeletal muscle fibre preparations, which were chemically or mechanically skinned. Interestingly, ECRE in these preparations consist of both spark-like and ember-like events, which could additionally occur in combination at the same location.

The present work aims to present and discuss the analysis of spark- and ember-like ECRE in skinned adult mammalian skeletal muscle fibres with a first and simplified spatio-temporal mathematical model of ECRE generation. It is based on a model which was originally developed for global Ca^{2+} transients (Uttenweiler et al. 1998) and which is now extended for studying ECRE in these preparations. Preliminary results of this work were presented at the World Congress on Cellular and Molecular Biology 2000 in Jena, Germany (Uttenweiler et al. 2000).

Materials and methods

The detailed description of the experimental conditions for recording ECRE in skinned skeletal muscle fibres can be found in Kirsch et al. (2001). A brief description of the microscopic recording conditions, the preparation and the solutions will be given in the following.

Confocal laser scanning microscopy

ECRE in skinned skeletal muscle fibres were measured in an experimental chamber, which was mounted on the stage of an inverted microscope (IX70, Olympus) and imaged through a 40× water immersion objective (UAPO40×W/340/1.15, Olympus). A confocal laser scanning unit (FV300, Olympus) was used to excite the Ca^{2+}-sensitive fluorescence indicator fluo-4 (60 μM) with the 488 nm line of a 20 mW Kr/Ar laser (Omnichrome, Melles Griot) and to record fluorescence emission at wavelengths larger than 510 nm using a barrier filter and a pinhole size of 150 μm. For the measurement of the dynamic morphological parameters of ECRE, confocal line scans were acquired with a temporal resolution of 2.05 ms per line. The point spread function (PSF) of the microscopic set-up was determined from the full width at half maximum (FWHM) of Gaussian fits applied to the lateral and axial intensity profiles of sub-resolution beads imaged in *xyz* stacks. The lateral and axial resolutions were 0.35 ± 0.02 μm and 1.06 ± 0.05 μm, respectively.

Preparations

All animals were handled according to the guidelines of the animal care committee of the University of Heidelberg. Single muscle fibres from the *extensor digitorum longus* (edl; fast twitch) of male Balb-C mice, sacrificed by a raising concentration of CO_2, were prepared in relaxing solution. Skinning was achieved by a 2 min application of 0.01 % saponin (Fluka) in relaxing solution, resulting in a selective perforation of the sarcolemma, or by mechanical removal of the outer membrane. For fluorescence imaging the fibres were fixed at both ends in the experimental chamber and immersed in the internal solution additionally containing 60 μM fluo-4.

Solutions

Total and free ion concentrations were calculated using the software program REACT II (obtained from G.L. Smith, University of Glasgow, Scotland). The following types of solution were used: relaxing solution: 140 mM K-glutamate, 10 mM HEPES, 5 mM glucose, 1 mM EGTA, 10 mM $MgCl_2$, 0.3 mM $CaCl_2$, pH 7.0; internal solution: 140 mM K-glutamate, 10 mM HEPES, 5 mM glucose, 0.5 mM EGTA, 5 mM Na_2ATP, 5 mM Na_2-creatine-phosphate, 5.4 mM $MgCl_2$, 0.1 mM $CaCl_2$, pH 7.0. The free Ca^{2+} concentration for the internal solution was 100 nM and the free Mg^{2+} concentration was 0.6 mM. All experiments were carried out at room temperature (22–23 °C).

Mathematical modelling

The model used for the simulation of ECRE is based on the mathematical model for global Ca^{2+} transients in skinned muscle fibres as described in Uttenweiler et al. (1998). For ECRE simulations the existing model has been expanded to a 2-D cylindrical geometry with radial symmetry. Thus, ion concentrations are calculated as a function of the radius r, the longitudinal coordinate z and time t. In general, the following processes are included in the model (see Fig. 1):

1. Diffusion of free Ca^{2+} ions, the fluorescent indicator fluo-4, EGTA, ATP and the respective Ca^{2+} complexes.
2. Diffusion of free Ca^{2+} ions in the longitudinal (z) direction inside the SR.
3. Ca^{2+} release by the SR through a source of variable extension.
4. Ca^{2+} re-uptake by the SR Ca^{2+} pumps.
5. Binding of Ca^{2+} ions inside the SR to calcium-binding proteins (CBP), pooled as a calsequestrin buffer.

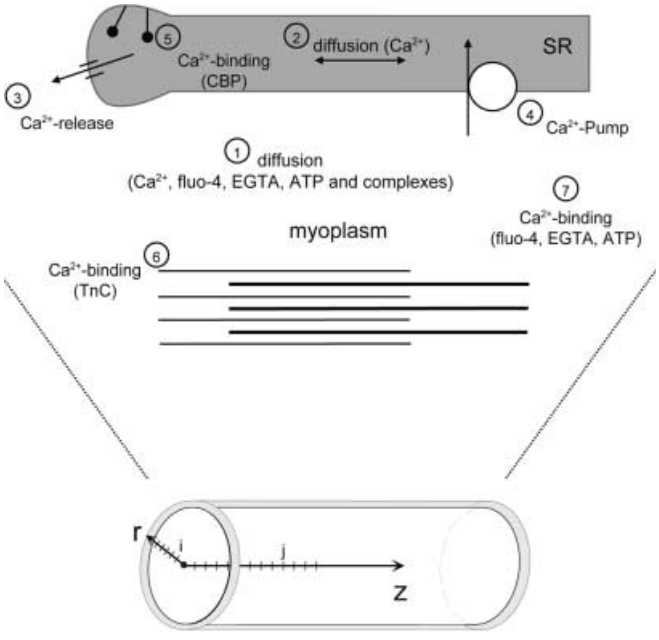

Fig. 1. Model geometry and the physiological processes included in the model. *1* Diffusion of free Ca^{2+} ions as well as diffusion of mobile buffers (fluo-4, EGTA, ATP) and their respective Ca^{2+} complexes in the myoplasm. *2* Diffusion of free Ca^{2+} ions inside the SR in longitudinal direction. *3* Ca^{2+} release and *4* re-uptake by the SR. Binding of Ca^{2+} ions to *5* Ca^{2+} binding proteins (CBP) inside the SR. *6* Binding to the immobile buffer TnC. *7* Binding to mobile buffers (fluo-4, EGTA, ATP). The muscle fibre is modelled in a cylindrical geometry with radial symmetry. The index for the spatial discretization in the radial (r) direction is denoted by i and in the longitudinal (z) direction by j

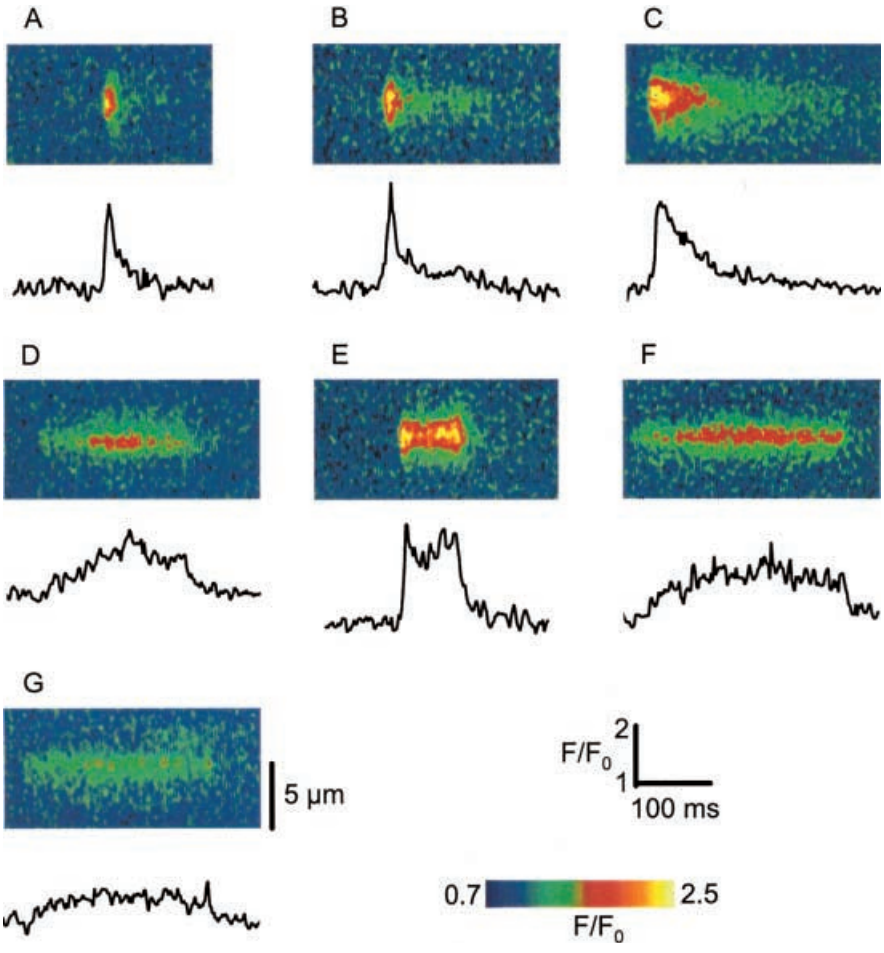

Fig. 2A–G. ECRE in skinned mammalian skeletal muscle fibres. The line scan images show typical examples for the variety of ECRE with spark-like events (**A**–**C**) and ember-like events (**D**–**G**). The morphological parameters are: **A**, amplitude 2.41 F/F_0, rise time 8.10 ms, FWHM 2.87 µm and FDHM 14.00 ms. **B**, amplitude 2.81 F/F_0, rise time 16.00 ms, FWHM 2.73 µm and FDHM 12.00 ms. **C**, amplitude 2.55 F/F_0, rise time 16.90 ms, FWHM 3.41 µm and FDHM 46.00 ms. **D**, amplitude 2.07 F/F_0, rise time 91.95 ms, FWHM 1.23 µm and FDHM 112.00 ms. **E**, amplitude 2.57 F/F_0, rise time 6.40 ms, FWHM 2.05 µm and FDHM 78.00 ms. **F**, amplitude 2.25 F/F_0, rise time 167.75 ms, FWHM 1.23 µm and FDHM 128.00 ms. **G**, amplitude 1.73 F/F_0, rise time 241.85 ms, FWHM 0.82 µm and FDHM 180.00 ms

6. Binding of Ca^{2+} ions to troponin-C.
7. Binding of Ca^{2+} ions to the mobile buffers fluo-4, EGTA and ATP.

The effect of soluble Ca^{2+} binding proteins is neglected, as the skinning leads to wash out of these Ca^{2+} buffers (Gillis 1985).

The model geometry has additionally been adopted such that the SR forms a compartment surrounding a myofibril which is used as the simulation volume. The SR interacts with the myofibrillar space by Ca^{2+} release from the Ca^{2+} source and an active Ca^{2+} re-uptake by the SR Ca^{2+}-ATPases. In this simplifying approach the very complex structure of the triadic region has been lumped together into a symmetric Ca^{2+} source centred at the cylinder axis. Additionally, the size of the source can be adjusted in both the radial and longitudinal spatial dimensions. Longitudinal diffusion of free Ca^{2+} ions inside the SR and binding to SR Ca^{2+} binding proteins with the kinetic properties of calsequestrin is also included in the model. The dimensions of the model volume are 1 µm in the radial and 2 µm in the longitudinal directions, respectively. The symmetry additionally leads to a mirroring of the model volume at $z=0$ µm.

The diffusion equation with the various source and sink terms in the 2-D cylindrical geometry can be written as (Crank 1975):

$$\frac{\partial c(r,z,t)}{\partial t} = \frac{1}{r}\frac{\partial}{\partial r}\left(rD\frac{\partial c(r,z,t)}{\partial r}\right) + \frac{\partial}{\partial z}\left(D\frac{\partial c(r,z,t)}{\partial z}\right) + h(r,z,t) \quad (1)$$

with the concentration c, the diffusion coefficient D and $h(r,z,t)$ being the sum of all source and sink terms of the various processes involved[1].

[1] $[Ca^{2+}]$ denotes the free Ca^{2+} concentration in the following equations

Ca^{2+} release

The release of Ca^{2+} ions from the SR is assumed to be proportional to the concentration gradient across the SR membrane:

$$\frac{d[Ca^{2+}]}{dt} = a_1\left([Ca^{2+}]_{SR} - [Ca^{2+}]_{myoplasm}\right) \text{ with } a_1 = a_1(r,z,t) \quad (2)$$

where $a_1(r,z,t)$ is a proportional constant which can be used for adjusting the extent of SR Ca^{2+} ion release per unit time.

Ca^{2+}-ATPase

The active removal of Ca^{2+} ions from the cytosol by the SR Ca^{2+} pump is modelled with a Hill-type relation, assuming a Ca^{2+}-dependent second-order saturable pump. The uptake of Ca^{2+} ions into the SR can then be written as:

$$\frac{d[Ca^{2+}]}{dt} = \frac{v_{max}[Ca^{2+}]^n}{[Ca^{2+}]^n + K_m^n} \quad (3)$$

where v_{max} is the maximum uptake velocity, K_m is the half-maximal uptake rate and $n=2$ is the Hill coefficient.

Buffers

Calcium is assumed to bind to all buffers in a 1:1 stoichiometry and without cooperativity, so that the following equation holds:

$$\frac{d[Ca^{2+}]}{dt} = \sum_{\ell} k_{on}^{\ell}[Ca^{2+}]_{free}[buffer^{\ell}]_{free} - k_{off}^{\ell}[Ca^{2+}\ buffer^{\ell}] \quad (4)$$

where ℓ denotes the various buffers, k_{on}^{ℓ} is the kinetic on-rate constant and k_{off}^{ℓ} is the kinetic off-rate constant of the buffer$^{\ell}$ Ca^{2+} binding. For the buffering of troponin-C, only the regulatory sites are considered. As the troponin concentration in skeletal muscle is roughly 70 μM (Gillis 1985) and each molecule has two regulatory binding sites, as a first approximation with no cooperativity the effective concentration can be taken as 140 μM. The high-affinity binding sites and the effect of Mg^{2+} competition are neglected in the model.

Discretization

The differential equations described above are solved using the method of explicit finite-differences. Let i and j denote the radial and the longitudinal grid positions, respectively, k the discrete time index, δr and δz the step-sizes in the radial and longitudinal directions, respectively, and δt the temporal step-size. Then, for the case of the diffusion equation the finite-difference approximation is given by:

$$\begin{aligned} c_{i,j,k+1} &= D\tfrac{\delta t}{2i(\delta r)^2}\{(2i+1)c_{i+1,j,k}+2ic_{i,j+1,k}-8ic_{i,j,k} \\ &\quad +(2i-1)c_{i-1,j,k}+2ic_{i,j-1,k}\}+c_{i,j,k} \quad for\ \ i\neq 0 \\ c_{0,j,k+1} &= D\tfrac{\delta t}{(\delta r)^2}\{4c_{1,j,k}-6c_{0,j,k}+c_{0,j+1,k}+c_{0,j-1,k}\}+c_{0,j,k} \quad for\ \ i=0 \end{aligned} \tag{5}$$

if additionally $\delta r = \delta z$, i.e. equal step-sizes in the radial and longitudinal directions. The model volume is divided into 50 intervals in the radial and 100 intervals in the longitudinal directions, leading to an effective spatial step-size of 20 nm for both spatial dimensions. The boundary of the system is treated with Neumann boundary conditions, i.e. zero perpendicular flux. For that case the explicit finite-difference formula is given by:

$$\begin{aligned} c_{i,j,k+1} &= D\tfrac{\delta t}{2i(\delta r)^2}\ \{2ic_{i,j+1,k}-(6i-1)c_{i,j,k} \\ &\quad +(2i-1)c_{i-1,j,k}+2ic_{i,j-1,k}\}+c_{i,j,k} \quad for\ \ i=i_{\max} \end{aligned} \tag{6}$$

The discretization for all other differential equations are implemented according to Uttenweiler et al. (1998).

Computing

The finite-difference algorithm was programmed in ANSI-C language and the calculations were performed using a R10000 workstation (Silicon Graphics, IRIX 6.4). The step-size for the time iteration was 4,000,000 time steps per second. The error in calculating the solution of the differential equations with the finite-difference algorithm was controlled by monitoring the amount of total Ca^{2+} in the model. Errors were kept below 1% in all calculations.

Simulation of the effect of the microscopic PSF

The experimentally detected fluorescence $F(x,y,z)$ is assumed to be the result of the convolution of the 3-D distribution of Ca^{2+} ions bound to the fluorescence indicator with the microscopic PSF:

$$\begin{aligned} F(x,y,z) = \iiint\ & [Ca^{2+}\text{fluo}-4](x',y',z') \\ & \text{PSF}(x-x',y-y',z-z')\,dx'\,dy'\,dz' \end{aligned} \tag{7}$$

Note that x, y, z are now Cartesian coordinates, with z being the optical axial direction of the microscope. We have simulated the PSF blurring by a convolution of the model output for the 3-D distribution of [Ca^{2+}fluo-4], which was explicitly calculated from the 2-D data of the model output, with a 3-D Gaussian kernel approximating the PSF:

$$\begin{aligned} F(x,y,z) &= \tfrac{(2\pi)^{-3/2}}{\sigma_x\sigma_y\sigma_z}\iiint [Ca^{2+}\text{fluo}-4](x',y',z') \\ &\quad \exp\left(-\left(\tfrac{(x-x')^2}{2\sigma_x^2}+\tfrac{(y-y')^2}{2\sigma_y^2}+\tfrac{(z-z')^2}{2\sigma_z^2}\right)\right)dx'\,dy'\,dz' \end{aligned} \tag{8}$$

The Gaussian kernel was chosen such that the spatial FWHMs correspond to the measured FWHMs of the PSF of our microscopic set-up (i.e. x-direction 350 nm, y-direction 350 nm, axial direction 1060 nm). The convolution was done in the spatial domain by additionally exploiting the separability of the 3-D Gaussian kernel into three independent 1-D Gaussian kernels to reduce the computational load (Jähne 1999):

$$\begin{aligned} F(x,y,z) &= \tfrac{(2\pi)^{-3/2}}{\sigma_x\sigma_y\sigma_z}\int\exp\left(-\tfrac{(x-x')^2}{2\sigma_x^2}\right)\int\exp\left(-\tfrac{(y-y')^2}{2\sigma_y^2}\right) \\ &\quad \int\exp\left(-\tfrac{(z-z')^2}{2\sigma_z^2}\right)[Ca^{2+}\text{fluo}-4](x',y',z')\,dz'\,dy'\,dx' \end{aligned} \tag{9}$$

Finally, the theoretical fluorescence $F(x,y,z)$ is normalized with the baseline fluorescence at time $t=0$ s, resulting in the normalized theoretical fluorescence F/F_0.

The results were stored such that theoretical line scan images at different sarcomeric locations could be directly compared to the experimentally obtained line scans.

Results

Typical line scan images of ECRE in skinned mammalian skeletal muscle fibre preparations are shown in Fig. 2. The fluorescence is expressed in normalized units (F/F_0). It is obtained from the ratio of the raw line scan data of fluorescence $F(x,t)$ and the average baseline fluorescence $F_0(x)$ prior to the event for every value of the temporal coordinate t. The spatial and temporal properties of the

Fig. 3A, B. Simulated line scan images of ECRE. The time courses of ECRE measured at the spatial coordinate of maximum amplitude are given below each image. **A** Panels S1–S3 show simulations of spark-type ECRE and S4–S6 of ember-like events. The following geometric and source parameters have been used in the simulations: *S1*, source size 40 nm in the r and z directions, duration of Ca^{2+} release 10 ms; *S2*, source size 40 nm in the r and z directions, duration of Ca^{2+} release 25 ms. *S3*, source size 40 nm in the r and 1 μm in the z directions, duration of Ca^{2+} release 10 ms; *S4*, source size 40 nm in the r and z directions, two-stage Ca^{2+} release with first stage duration of 10 ms followed by a second stage of 90 ms; *S5*, source size 40 nm in the r and z directions, two-stage Ca^{2+} release with first duration of 20 ms and second of 180 ms; *S6*, source size 40 nm in the r and z directions, one-stage Ca^{2+} release with 62.5 ms duration. The morphological parameters are: *S1*, amplitude 4.98 F/F_0, FDHM 20 ms, rise time 7.5 ms; *S2*, amplitude 5.64 F/F_0, FDHM 47.5 ms, rise time 22.5 ms; *S3*, amplitude 4.65 F/F_0, FDHM 20 ms, rise time 7.5 ms; *S4*, amplitude 3.83 F/F_0, FDHM 120 ms, rise time 10 ms; *S5*, amplitude 3.25 F/F_0, FDHM 218 ms, rise time 17.5 ms; *S6*, amplitude 4.28 F/F_0, FDHM 90 ms, rise time 57.5 ms. **B** Panels *S1Ca–S6Ca* show the corresponding free Ca^{2+} ion concentrations of the simulated line scans S1–S6, respectively. Note: the spatial coordinate has been expanded in order to visualize the narrow spatial distribution of free Ca^{2+} ions in more detail. Additionally, the colour coding has been chosen such that it is consistent for all six panels. For panels S1Ca and S2Ca this leads to a colour saturation at the peak concentrations. The morphological parameters are: *S1Ca*, amplitude 159 μM, FDHM 10 ms, rise time 0.6 ms; *S2Ca*, amplitude 159 μM, FDHM 25 ms, rise time 0.6 ms; *S3Ca*, amplitude 18.6 μM, FDHM 10 ms, rise time 0.6 ms; *S4Ca*, amplitude 68.6 μM, FDHM 7.5 ms, rise time 2.5 ms; *S5Ca*, amplitude 45.3 μM, FDHM 20 ms, rise time 1.25 ms; *S6Ca*, amplitude 43.9 μM, FDHM 62.5 ms, rise time 1.25 ms

ECRE are characterized by four event parameters: amplitude (maximum increase in fluorescence), FWHM (measured at the time of the peak), full duration at half maximum (FDHM) and rise time (elapsed between 10% and full amplitude at the spatial centre). As described in Kirsch et al. (2001), ECRE in these preparations consist of spark-like events (panels A–C), ember-like events (panels D–G) and combinations thereof. Interestingly, this is a major difference to amphibian skinned muscle fibre preparations, where only Ca^{2+} sparks could be detected. Typical values of the morphological parameters of mammalian ECRE are in the range 1.5–4.5 F/F_0 for the amplitude and 1.2–3.0 μm for the FWHM. For spark-like events the typical temporal morphological parameters are 8–18 ms for the rise time and 10–49 ms for the FDHM, whereas for ember-like events the rise times are in the range 15–250 ms and FDHM in the range 50–350 ms. The morphological parameters of the ECRE shown in Fig. 2 are given in the figure legend. The greater variability of mammalian ECRE time courses and spatial properties exemplarily demonstrated in Fig. 2 /FIGREF > suggest that additional control factors of Ca^{2+} release are involved in mammalian compared to amphibian skeletal muscle preparations.

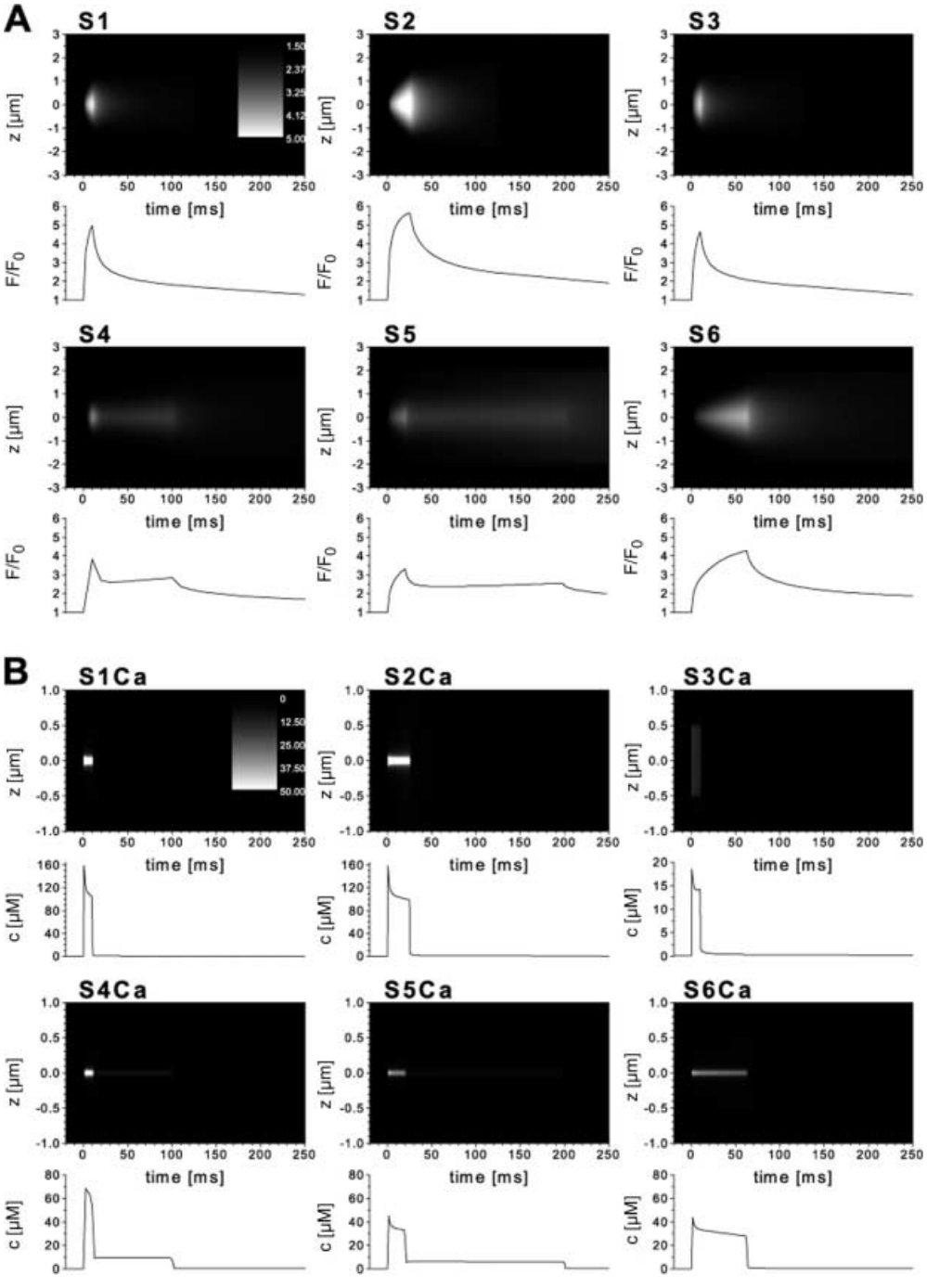

The output of the model calculations for simulated line scan images obtained under various assumptions and conditions is shown in Fig. 3. The simulations in panels S1–S3 correspond to spark-like events. The source size in the model calculations for S1 and S2 is 40 nm in both the radial and longitudinal directions and the period of Ca^{2+} release is 10 ms in S1 and 25 ms in S2. In the simulation shown in panel S3 the source size is 40 nm in the radial and 1 μm in the longitudinal directions and the source is open for 10 ms. With these settings, spark-like events with different time courses and spatial properties can be effectively simulated. The simulation of ember-like events is shown in panels S4–S6. The source size is 40 nm in both the radial and longitudinal directions for all three simulations and Ca^{2+} release is modelled either as a two-stage release (S4, S5) or a one-stage release (S6) with a source open time of 62.5 ms. The two-stage release is obtained by an initial opening of the source for 10 ms (S4) and 20 ms (S5), followed by the second opening of 90 ms (S4) and 180 ms (S5) with a reduced proportionality factor a_1 in Eq. (2). In simulation S4, a_1 was reduced by a factor of 10 and in simulation S5 it was reduced by a factor of 14. The situation of a two-stage source basically corresponds to either changes in single-channel conductances or changes in channel recruitment during ECRE, as discussed by González et al. (2000) for experiments with drug-modulated amphibian Ca^{2+} sparks.

In addition to the simulated line scan images, the corresponding free Ca^{2+} ion distributions are given in panels S1Ca–S6Ca. The free Ca^{2+} ion distribution turns out to be much more confined in space and it also exhibits more rapid decay characteristics than the fluorescence signal. Both effects are due to the lack of equilibrium between the fluorescent indictor and the free Ca^{2+} ions and to the large spatial concentration gradients, as discussed in Smith et al. (1998).

The detailed spatio-temporal characteristics of the simulated ECRE are summarized in the time course traces of Fig. 3, and in Figs. 4 and 5 for the spark-like and ember-like ECRE, respectively. The variety of experimentally observed spark-like ECRE can be modelled by varying the open times of the Ca^{2+} source in the range 5–30 ms. Interestingly, the duration of Ca^{2+} release shows a larger effect on ECRE spatial dimensions (FWHM) than the actual source size in the longitudinal (z) direction. This can be seen in Fig. 4A, where the FWHM of the ECRE with a 40 nm point source and 25 ms release time is 2.12 μm, in comparison to a FWHM of 1.56 μm for the ECRE with a 1 μm source opened for 10 ms. The release currents in panel C indi-

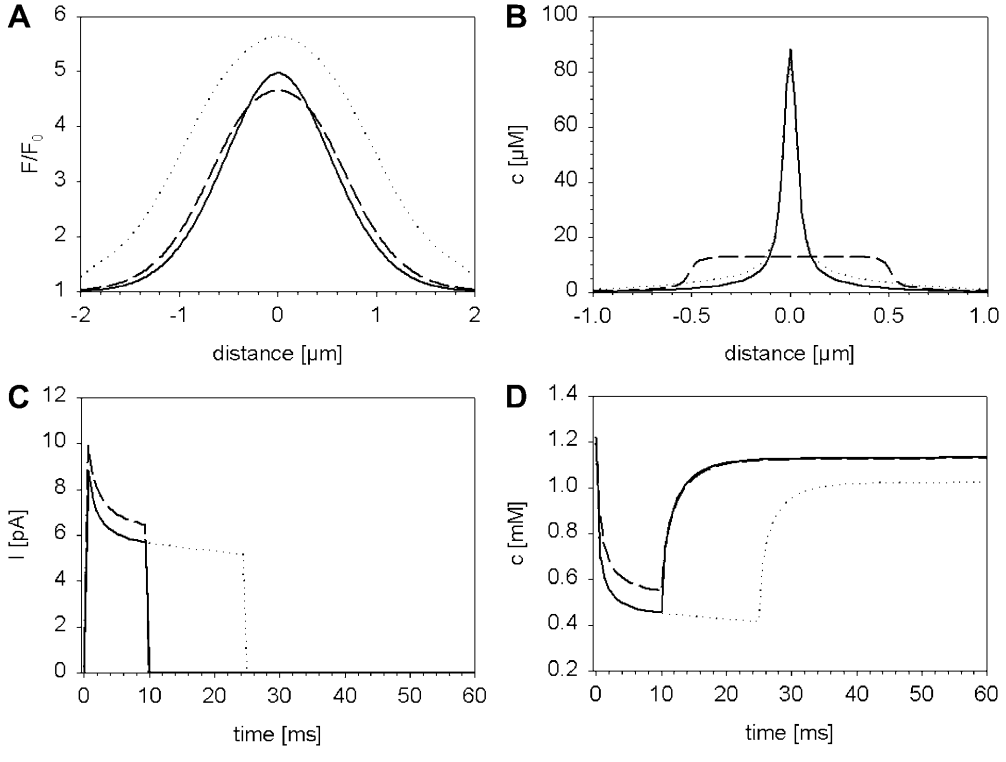

Fig. 4A–D. Simulated spatial and temporal ECRE properties of spark-like events. The *solid lines* correspond to simulation S1 in Fig. 3, the *dotted lines* to S2 and the *dashed lines* to S3, respectively. **A** Spatial profile of ECRE measured at the temporal coordinate of maximum amplitude. **B** Spatial profile of the free Ca^{2+} ion concentration measured at the temporal coordinate of maximum amplitude F/F_0 of the simulated line scan images. Note that there is a distinct difference of the time in peak amplitude for the line scan images and the free Ca^{2+} ion concentration, which can be seen in the respective time courses of Fig. 3. **C** Ca^{2+} release current from the SR. **D** Average free Ca^{2+} ion concentration inside the SR. The average was calculated from the SR concentrations between $z=0$ μm and $z=0.6$ μm. The morphological parameters are: S1, FWHM 1.32 μm (*solid line*); S2, FWHM 2.12 μm (*dotted line*); S3, FWHM 1.56 μm (*dashed line*); S1Ca, FWHM 0.12 μm (*solid line*); S2Ca, FWHM 0.12 μm (*dotted line*); S3Ca, FWHM 1.04 μm (*dashed line*)

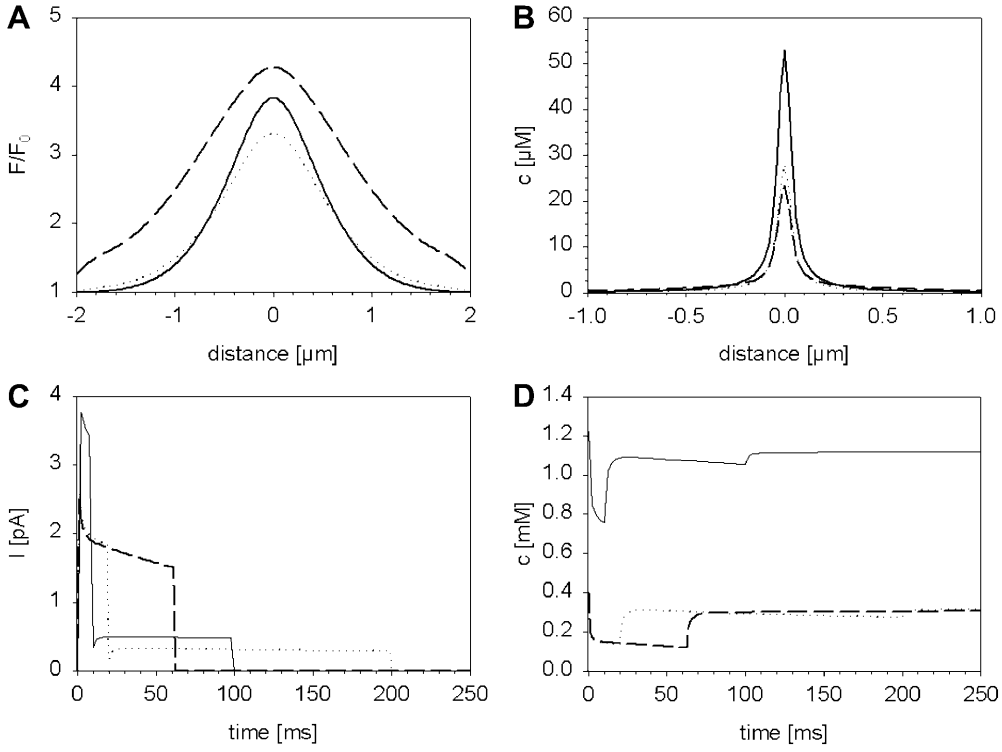

Fig. 5A–D. Simulated spatial and temporal ECRE properties of ember-like events. The panels are analogous to Fig. 4. The *solid lines* correspond to simulation S4 in Fig. 3, the *dotted lines* to S5 and the *dashed lines* to S6, respectively. The morphological parameters are: S4, FWHM 1.1 µm (*solid line*); S5, FWHM 1.32 µm (*dotted line*); S6, FWHM 1.84 µm (*dashed line*); S4Ca, FWHM 0.10 µm (*solid line*); S5Ca, FWHM 0.08 µm (*dotted line*); S6Ca, FWHM 0.08 µm (*dashed line*)

cate that, for the assumption of a Ca^{2+} release which is proportional to the free Ca^{2+} gradient across the SR membrane, the release current is not constant in time, even during short spark-like events. In previous models of amphibian skeletal muscle, Ca^{2+} sparks (Jiang et al. 1999; Ríos et al. 1999), cardiac myocytes (Smith et al. 1998) and general spark models (Izu et al. 1998), the release current was assumed constant during Ca^{2+} sparks. The time course of the averaged free Ca^{2+} concentration in the longitudinal distance z = 0–0.6 µm inside the SR in panel D yields the explanation for the declining Ca^{2+} release current. For the parameter values of SR Ca^{2+} buffer binding summarized in Table 1, the free Ca^{2+} ion concentration inside the SR significantly declines in the first 5 ms of the Ca^{2+} release. The dissociation of Ca^{2+} ions bound to the luminal Ca^{2+} buffer calsequestrin in the small SR volume and longitudinal diffusion of Ca^{2+} ions is not fast enough to compensate for the loss of Ca^{2+} ions during the initial release phase. Upon termination of Ca^{2+} release the free Ca^{2+} ion concentration regenerates in less than 5 ms to nearly the original value. The detailed spatio-temporal profile of the free Ca^{2+} ion concentration inside the SR during the spark-like event S1 is shown in Fig. 6. It can be clearly seen that the free Ca^{2+} ion concentration significantly decreases during the event, even at a distance of 2 µm from the Ca^{2+} source.

The simulations of the ember-like ECRE were accomplished by either a one-stage or a two-stage source, as explained above. With these assumptions, ember-like ECRE could be reproduced as seen in Figs. 3 and 5. However, it was not possible to simulate ember-like events with steady fluorescence levels at low amplitudes, e.g. as shown in Fig. 2G. Also, the simulated ember-like events were all preceded by an overshoot in the rising phase. From the time courses in Fig. 3 it is difficult to distinguish if experimentally observed ember-like events are due to a one-stage, a two-stage or even a different release mode. These events also cannot be explained by out-of-focus release events, as simulated line scan images with different distances to the release site did not reproduce events with a steady low amplitude.

Additionally, we found that changing the initial free Ca^{2+} ion concentration inside the SR (from 1.2 mM to 0.4 mM) did not significantly alter the ECRE properties, as seen from the time courses of simulation S4 in comparison to S5. Interestingly, as for spark-like events, we found that the spatial spread of the event is mostly dependent on the duration of the first-stage Ca^{2+} release current with the larger proportionality factor a_1. This observation is in agreement with Izu et al. (2001), who found that mainly the amplitude of the Ca^{2+} release current determines the spatial spread of Ca^{2+} sparks in their model.

Discussion

The discovery of ECRE in skinned fibre preparations of adult mammalian skeletal muscle has opened many new and exciting questions in skeletal muscle EC coupling. Especially, the morphological variety of ECRE in mammals in comparison to the stereotype appearance of Ca^{2+} sparks in amphibians suggests that additional control factors of Ca^{2+} release are involved in mammals. In order to address this question, we have presented here the approach of a model-based analysis of

Table 1. Parameters used in the simulations

Definition	Standard value	Source
Calcium diffusion		
Cytosolic diffusion coefficient	$D_{Ca} = 350\ \mu m^2\ s^{-1}$	Wagner and Keizer (1994)
Sarcoplasmic reticulum		
Resting free Ca^{2+} concentration	$c^{SR}_{Ca\text{-}rest} = 0.4$–$2$ mM	Cannell and Allen (1984)
Local CS binding site concentration	$c^{CS}_{tot} = 31$ mM	Cannell and Allen (1984)
Kinetic on- and off-rate constants, CS-Ca^{2+}	$k_{on} = 8772\ M^{-1}\ s^{-1}$, $k_{off} = 10\ s^{-1}$	Donoso et al. (1995)
Dissociation constant, CS-Ca^{2+}	$K_d = 1.14$ mM	Donoso et al. (1995)
SR Ca^{2+} pump		
Maximum uptake rate	$v_{max} = 60\ \mu M\ s^{-1}$	Stienen et al. (1995)
Half maximal rate	$k_m = 0.24\ \mu M$	Stienen et al. (1995)
Hill coefficient	$n = 2.07$	Stienen et al. (1995)
TnC regulatory sites		
Total local concentration	$c^{TnC} = 140\ \mu M$	Robertson et al. (1981)
Kinetic on- and off-rate constants, TnC-Ca^{2+}	$k_{on} = 1.2\times10^8\ M^{-1}\ s^{-1}$, $k_{off} = 23\ s^{-1}$	Robertson et al. (1981)
Dissociation constant, TnC-Ca^{2+}	$K_d = 0.2\times10^{-6}$ M	Robertson et al. (1981)
ATP		
Dissociation constant, ATP-Ca^{2+}	$K_d = 200\ \mu M$	Baylor and Hollingworth (1998)
Kinetic on- and off-rate constants, ATP-Ca^{2+}	$k_{on} = 150\times10^6\ M^{-1}\ s^{-1}$, $k_{off} = 30{,}000\ s^{-1}$	Baylor and Hollingworth (1998)
Cytosolic diffusion coefficient	$D_{ATP} = 140\ \mu m^2\ s^{-1}$	Baylor and Hollingworth (1998)
EGTA		
Dissociation constant, EGTA-Ca^{2+}	$K_d = 0.627\ \mu M$ [a]	Pape et al. (1995)
Kinetic on- and off-rate constants, EGTA-Ca^{2+}	$k_{on} = 1.5\times10^6\ M^{-1}\ s^{-1}$, $k_{off} = 0.94\ s^{-1}$ [a]	Pape et al. (1995)
Cytosolic diffusion coefficient	$D_{EGTA} = 170\ \mu m^2\ s^{-1}$	Pape et al. (1995)
Fluo-4		
Dissociation constant, fluo-Ca^{2+}	$K_d = 0.74\ \mu M$	Escobar et al. (1997)
Kinetic on- and off-rate constants, fluo-Ca^{2+}	$k_{on} = 236\times10^6\ M^{-1}\ s^{-1}$, $k_{off} = 175\ s^{-1}$	Escobar et al. (1997)
Cytosolic diffusion coefficient	$D_{fluo\text{-}4} = 200\ \mu m^2\ s^{-1}$	Harkins et al. (1993)

[a]Strongly dependent on pH variation; value for pH 7.0

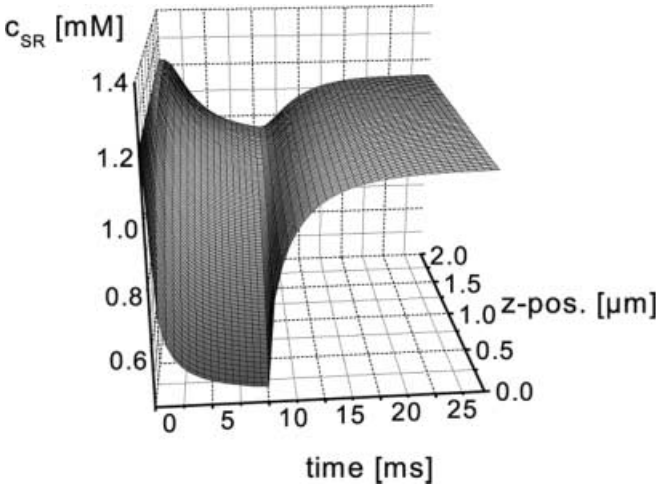

Fig. 6. Free Ca^{2+} ion concentration inside the SR. The free Ca^{2+} ion concentration inside the SR during the spark-like event S1 in Fig. 3 is plotted versus the longitudinal coordinate z and time t. It can be clearly seen that the free Ca^{2+} ion concentration significantly decreases during the event, even at a distance of 2 µm

ECRE in skinned mammalian skeletal muscle fibre preparations. In this first and simplified modelling approach we could reconstruct the basic morphological parameters of ECRE. However, it also became clear that, especially for the modelling of ember-like ECRE, the current mathematical models are still not sufficiently detailed enough to successfully reconstruct all features of ECRE, especially those with prolonged stable low-amplitude time courses. The spatial spread of ECRE was found to be higher correlated to source open times and release currents (Izu et al. 2001) than to source widths examined up to 1 µm. Such large longitudinal source extensions would additionally be very unlikely from structural data, as discussed in Ríos et al. (1999).

One major result of the present work is that under our model assumptions a depletion of luminal free Ca^{2+} concentration is predicted even for short spark-like events. Such a depletion could be an essential factor of intraluminal control of SR Ca^{2+} release. Studies on triads isolated from mammalian skeletal muscle (Donoso et al. 1995) showed that luminal Ca^{2+} concentration had a distinctive effect on Ca^{2+} release, presumably by regulating SR calcium channels. Additionally, there were profound differences between amphibian and mammalian preparations. Lipid bilayer experiments also suggest a regulation of RyR by luminal Ca^{2+} sensing sites (Gyorke and Gyorke 1998; Ching et al. 2000). This intraluminal regulation in conjunction with luminal Ca^{2+} depletion could also serve as a factor involved in ECRE termination, in addition to membrane potential and hence DHP-RyR mediated termination (Lacampagne et al. 2000). However, the influence of the luminal Ca^{2+} concentration on ECRE has been mainly studied for the

RyR2 isoform in cardiac muscle and is still controversially discussed. In ventricular myocytes there has been no experimental evidence for a physiological role of intraluminal Ca^{2+} depletion for ECRE termination (Lukyanenko et al. 1998) or activation (Song et al. 1997).

In general, our study shows that it is most essential to develop more sophisticated mathematical models, which include the known structural and functional molecular details. In a further extension of our model, the complex morphological structure of triads has to be treated in its entire 3-D topology in order to fully understand the effects of restricted volumes and the molecular arrangements of Ca^{2+} release units. It should be noted that in mammals the situation is even more complex than in amphibian skeletal muscle, since there are two segments of TTS per sarcomere. Also, especially for mammalian skeletal muscle it is essential to include the details of the complex molecular DHP-RyR interaction in order to allow a reliable feedback from model calculations. Additionally, other Ca^{2+} ion stores, e.g. mitochondria, which are directly or indirectly involved in cellular and subcellular Ca^{2+} handling, have to be included in further models as they might play an important role in ECRE modulation. These demands also require new and effective concepts for sophisticated spatio-temporal mathematical models, including the possibility of solving differential equations on the exact cellular and sub-cellular 3-D topology and methods of scale transitions from molecular processes in the ångström and femtosecond range to the cellular responses in the micrometer and millisecond range.

For the necessary combined experimental and mathematical modelling concept, skinned muscle fibre preparations can help to elucidate the mechanisms involved in the complex mechanism of mammalian ECRE generation, since the direct diffusional access to the myoplasm allows studies under strictly controlled intracellular conditions.

Acknowledgements This work was supported by grants from the Deutsche Forschungsgemeinschaft (FOR240/3-1) and BMBF 13N7871.

References

Baylor SM, Hollingworth S (1998) Model of sarcomeric Ca^{2+} movements, including ATP Ca^{2+} binding and diffusion, during activation of frog skeletal muscle. J Gen Physiol 112:297–316

Block BA, Imagawa T, Campbell KP, Franzini-Armstrong C (1988) Structural evidence for direct interaction between the molecular components of the transverse tubule/sarcoplasmic reticulum junction in skeletal muscle. J Cell Biol 107:2587–2600

Cannell MB, Allen DG (1984) Model of calcium movement during activation in the sarcomere of frog skeletal muscle. Biophys J 45:913–925

Cheng H, Lederer WJ, Cannell MB (1993) Calcium sparks: elementary events underlying excitation-contraction coupling in heart muscle. Science 262:740–744

Ching LL, Williams AJ, Sitsapesan R (2000) Evidence for Ca(2+) activation and inactivation sites on the luminal site of the cardiac ryanodine receptor complex. Circ Res 87:201–206

Conklin MW, Ahern CA, Vallejo P, Sorrentino V, Takeshima H, Coronado R (2000) Comparison of Ca(2+) sparks produced independently by two ryanodine receptor isoforms (type 1 or type 3). Biophys J 78:1777–1785

Crank J (1975) The mathematics of diffusion. Oxford University Press, Oxford

Donoso P, Prieto H, Hidalgo C (1995) Luminal calcium regulates calcium release in triads isolated from frog and rabbit skeletal muscle. Biophys J 68:507–515

Dulhunty AF (1992) The voltage-activation of contraction in skeletal muscle. Prog Biophys Mol Biol 57:181–223

Escobar AL, Velez P, Kim AM, Cifuentes F, Fill M, Vegara JL (1997) Kinetic properties of DM-nitrophen and calcium indicators: rapid transient response to flash photolysis. Pflügers Arch 434:615–631

Gillis JM (1985) Relaxation of vertebrate skeletal muscle. A synthesis of the biochemical and physiological approaches. Biochim Biophy Acta 811:97–145

González A, Kirsch WG, Shirokova N, Pizarro G, Brum G, Pessah IN, Stern MD, Cheng H, Ríos E (2000) Involvement of multiple intracellular release channels in calcium sparks of skeletal muscle. Proc Natl Acad Sci USA 97:4380–4385

Gyorke I, Gyorke S (1998) Regulation of the cardiac ryanodine receptor channel by luminal Ca^{2+} involves luminal Ca^{2+} sensing sites. Biophys J 75:2801–2810

Harkins AB, Kurebayashi N, Baylor SM (1993) Resting myoplasmic free calcium in frog skeletal muscle fibres estimated with fluo-3. Biophys J 65:865–881

Izu LT, Wier WG, Balke CW (1998) Theoretical analysis of Ca^{2+} spark amplitude. Biophys J 75:1144–1162

Izu LT, Mauban JRH, Balke CW, Wier WG (2001) Large currents generate cardiac Ca^{2+} sparks. Biophys J 80:88–102

Jähne B (1999) Spatial and Fourier domain. In: Jähne B, Haussecker H, Geissler P (eds) Handbook of computer vision and applications, vol 2. Academic Press, San Diego, pp 35–66

Jiang YH, Klein MG, Schneider MF (1999) Numerical simulation of Ca^{2+} "sparks" in skeletal muscle. Biophys J 77:2333–2357

Kirsch WG, Uttenweiler D, Fink RHA (2001) Spark- and ember-like elementary Ca^{2+} release events in skinned fibres of adult mammalian skeletal muscle. J Physiol (Lond) 537:379–389

Klein MG, Cheng H, Santana LF, Jiang YH, Lederer WJ, Schneider MF (1996) Two mechanisms of quantized calcium release in skeletal muscle. Nature 379:455–458

Lacampagne A, Klein MG, Ward CW, Schneider MF (2000) Two mechanisms for termination of individual Ca^{2+} sparks in skeletal muscle. Proc Natl Acad Sci USA 97:7823–7828

Lipp P, Niggli E (1998) Fundamental calcium release events revealed by two-photon excitation photolysis of caged calcium in guinea-pig cardiac myocytes. J Physiol (Lond) 508:801–809

Lukyanenko V, Wiesner TF, Gyorke S (1998) Termination of Ca^{2+} release during Ca^{2+} sparks in rat ventricular myocytes. J Physiol (Lond) 507:667–677

Nelson MT, Cheng H, Rubart M, Santana LF, Bonev AD, Knot HJ, Lederer WJ (1995) Relaxation of arterial smooth muscle by calcium sparks. Science 270:633–637

Pape PC, Jong DS, Chandler WK (1995) Calcium release and its voltage dependence in frog cut muscle fibres equilibrated with 20 mM EGTA. J Gen Physiol 106:259–336

Ríos E, Brum G (1987) Involvement of dihydropyridine receptors in excitation-contraction coupling in skeletal muscle. Nature 325:717–720

Ríos E, Stern MD, González A, Pizarro G, Shirokova N (1999) Calcium release flux underlying Ca^{2+} sparks of frog skeletal muscle. J Gen Physiol 114:31–48

Robertson SP, Johnson JD, Potter JD (1981) The time-course of Ca^{2+} exchange with calmodulin, troponin, parvalbumin, and myosin in response to transient increases in Ca^{2+}. Biophys J 34:554–569

Shirokova N, Garcia J, Ríos E (1998) Local calcium release in mammalian skeletal muscle. J Physiol (Lond) 512:377–384

Smith GD, Keizer JE, Stern MD, Lederer WJ, Cheng H (1998) A simple numerical model of calcium spark formation and detection in cardiac myocytes. Biophys J 75:15–32

Song L-S, Stern MD, Lakatta EG, Cheng H (1997) Partial depletion of sarcoplasmic reticulum calcium does not prevent calcium sparks in rat ventricular myocytes. J Physiol (Lond) 505:665–675

Stienen GJM, Zaremba R, Elzinga G (1995) ATP utilization for calcium uptake and force production in skinned muscle fibres of *Xenopus laevis*. J Physiol (Lond) 482:109–122

Tsugorka A, Ríos E, Blatter L (1995) Imaging elementary events of calcium release in skeletal muscle cells. Science 269:1723–1726

Uttenweiler D, Weber C, Fink RHA (1998) Mathematical modelling and fluorescence imaging as a new approach to study the Ca^{2+} turnover in skinned muscle fibres. Biophys J 74:1640–1653

Uttenweiler D, Kirsch W, Schulzke E, Fink RHA (2000) Model based fluorescence imaging of elementary Ca^{2+}-release events: from single ion channels to molecular assemblies. 46th Cellular and Molecular Biology Congress, Jena, Germany, Abstract 253

Wagner J, Keizer J (1994) Effects of rapid buffers on Ca^{2+} diffusion and Ca^{2+} oscillations. Biophys J 67:447–456